# Role of the $\Delta$ resonance in the population of a four-nucleon state in the $^{56}$Fe $\rightarrow$ $^{54}$Fe reaction at relativistic energies

Zs. Podolyák,[1] C.M. Shand,[1] N. Lalović,[2,3] J. Gerl,[3] D. Rudolph,[2] T. Alexander,[1] P. Boutachkov,[3] M.L. Cortés,[3,4] M. Górska,[3] I. Kojouharov,[3] N. Kurz,[3] C. Louchart,[4] E. Merchán,[4] C. Michelagnoli,[5] R.M. Pérez-Vidal,[6] S. Pietri,[3] D. Ralet,[4,3] M. Reese,[4] H. Schaffner,[3] Ch. Stahl,[4] H. Weick,[3] F. Ameil,[3] G. de Angelis,[7] T. Arici,[3,8] R. Carroll,[1] Zs. Dombrádi,[9] A. Gadea,[6] P. Golubev,[2] M. Lettmann,[4] C. Lizarazo,[4,3] J. Mahboub,[10] H. Pai,[4] Z. Patel,[1] N. Pietralla,[4] P.H. Regan,[1] L.G. Sarmiento,[2] O. Wieland,[11] E. Wilson,[1] B. Birkenbach,[12] B. Bruyneel,[13] I. Burrows,[14] L. Charles,[15] E. Clément,[5] F. C. L. Crespi,[16,11] D.M. Cullen,[17] P. Désesquelles,[18] J. Eberth,[12] V. González,[19] T. Habermann,[4,3] L. Harkness-Brennan,[20] H. Hess,[12] D.S. Judson,[20] A. Jungclaus,[21] W. Korten,[13] M. Labiche,[14] A. Maj,[22] D. Mengoni,[23,24] D. R. Napoli,[7] A. Pullia,[16,11] B. Quintana,[25] G. Rainovski,[26] P. Reiter,[12] M.D. Salsac,[13] E. Sanchis,[19] and J.J. Valiente Dóbon[7]

[1] *Department of Physics, University of Surrey, Guildford, GU2 7XH, UK*
[2] *Department of Physics, Lund University, S-22100 Lund, Sweden*
[3] *GSI Helmholtzzentrum für Schwerionenforschung GmbH, D-64291 Darmstadt, Germany*
[4] *Institut für Kernphysik, TU Darmstadt, D-64289 Darmstadt, Germany*
[5] *GANIL, CEA/DRF-CNRS/IN2P3, F-14076 Caen Cedex 05, France*
[6] *Instituto de Fisica Corpuscular, Universitat de Valencia, E-46980 Valencia, Spain*
[7] *INFN, Laboratori Nazionali di Legnaro, I-35020 Legnaro, Italy*
[8] *Justus-Liebig-Universität Giessen, D-35392 Giessen, Germany*
[9] *Institute for Nuclear Research, Hungarian Academy of Sciences, P.O. Box 51, Debrecen, H-4001, Hungary*
[10] *Physics Department, University of Hail, PO Box 2440, Hail, KSA*
[11] *INFN, Sezione di Milano, I-20133 Milano, Italy*
[12] *Institut für Kernphysik, Universität zu Köln, D-50937 Köln, Germany*
[13] *Irfu, CEA, Université Paris-Saclay, F-91191 Gif-sur-Yvette, France*
[14] *STFC Daresbury Laboratory, Daresbury, Warrington, WA4 4AD, UK*
[15] *Institut Pluridisciplinaire Hubert Curien, CNRS-IN2P3, Université de Strasbourg, F-67037 Strasbourg, France*
[16] *Dipartimento di Fisica dell'Università degli Studi di Milano, I-20133 Milano, Italy*
[17] *School of Physics and Astronomy, Schuster Laboratory, University of Manchester, Manchester M13 9PL, UK*
[18] *Centre de Spectrométrie Nucléaire et de Spectrométrie de Masse - CSNSM, CNRS/IN2P3 and Univ. Paris-Sud, F-91405 Orsay Campus, France*
[19] *Department of Electronic Engineering, University of Valencia, E-46100 Burjassot (Valencia), Spain*
[20] *Oliver Lodge Laboratory, The University of Liverpool, Liverpool, L69 7ZE, UK*
[21] *Instituto de Estructura de la Materia, CSIC, Madrid, E-28006 Madrid, Spain*
[22] *Institute of Nuclear Physics Polish Academy of Sciences, PL-31-342 Krakow, Poland*
[23] *Dipartimento di Fisica e Astronomia dell'Università degli Studi di Padova, I-35131 Padova, Italy*
[24] *INFN, Sezione di Padova, I-35131 Padova, Italy*
[25] *Laboratorio de Radiaciones Ionizantes, Universidad de Salamanca, E-37008 Salamanca, Spain*
[26] *Faculty of Physics, St. Kliment Ohridski University of Sofia, 1164 Sofia, Bulgaria*

(Dated: September 14, 2016)

The $^{54}$Fe nucleus was populated from a $^{56}$Fe beam impinging on a Be target with an energy of $E/A$=500 M eV. The internal decay via $\gamma$-ray emission of the $10^+$ metastable state was observed. As the structure of this isomeric state has to involve at least four unpaired nucleons, it cannot be populated in a simple two-neutron removal reaction from the $^{56}$Fe ground state. The isomeric state was produced in the low-momentum/energy tail of the parallel momentum/energy distribution of $^{54}$Fe, suggesting that it was populated via the decay of the $\Delta^0$ resonance into a proton. This process allows the population of four-nucleon states, such as the observed isomer. Therefore, it is concluded that the observation of this $10^+$ metastable state in $^{54}$Fe is a consequence of the quark structure of the nucleons.

PACS numbers: 25.75.Ag, 25.40.Kv, 29.30.Kv, 27.40.+z

*Introduction:* The structure of atomic nuclei can be understood considering the interaction between its constituents, protons and neutrons. The properties of nuclear states, being of single-particle or collective type, are always expressed in terms of proton and neutron excitations. Although nucleons are not elementary particles, their inner structure usually does not have to be considered in order to explain the low-energy nuclear properties. One exception is the magnetic moment of the nucleus, where the non zero value in the case of the neu-

tron [1] and the unexpectedly large value for proton [2] provided early evidences that nucleons are composite, not elementary, particles.

The nucleons, protons and neutrons, consist of three quarks [3, 4]. The lowest energy excitation of a nucleon is the $\Delta$ resonance at an energy of 1232 MeV [5]. The $\Delta$ resonance of a proton, $\Delta^+$, can decay into a proton ($\Delta^+ \rightarrow \pi^0 + p$), or into a neutron ($\Delta^+ \rightarrow \pi^+ + n$). Similarly, the $\Delta$ resonance of a neutron, $\Delta^0$, can decay into a neutron ($\Delta^0 \rightarrow \pi^0 + n$), or into a proton ($\Delta^0 \rightarrow \pi^- + p$). The fact that the $\Delta$ resonance plays a role in relativistic-energy charge-exchange reactions was established, by studying the final ejectile nuclei, in the 1980's [6].

Here we present results of an experiment where the population of an *excited state* of a nucleus is the consequence of the inner quark structure of the nucleon. The nucleus of interest was populated in relativistic-energy heavy-ion collision.

Understanding relativistic-energy reactions [7] is in itself important for several reasons. It forms the basis of existing and future radioactive-beam facilities [8, 9], as it is one of the main processes to produce previously unidentified nuclear species [10]. It is also the mechanism which explains the nucleosynthesis of the chemical elements beryllium, boron and possibly lithium [11]. These elements are not produced in the stars, but from the fragmentation of carbon and oxygen in the interstellar medium.

We define relativistic-energy reactions, those which occurs during the collision between two nuclei at relative velocities higher than the Fermi velocity of the nucleons ($v_F \sim 10^6$ m/s). Peripheral collisions, resulting in fragments with masses close to those of the projectile and target, can be described rather successfully by the two-step abrasion-ablation model [12, 13]. The macroscopic abrasion model, the most successful so far, relies on the concept of a clean cut of the projectile nucleus by the target (and *vice versa*). According to the model, since the relative velocity of the reaction partners is much higher than $v_F$, the nucleon-nucleon collisions are restricted to the overlap zone. The parts of the nuclei outside the overlap zone, called spectators or prefragments, are not supposed to be affected in the abrasion process. Considering nucleons as elementary particles, as in both abrasion and ablation phases nucleons are removed, the reaction products will always have fewer or equal number of protons and neutrons than the initial nucleus. Therefore the product will be a fragment of the initial nucleus. Accordingly, we adopt the term fragmentation for this process in the present letter. We include in this term direct processes such as one or multi-nucleon removals (sometimes called cold fragmentation).

The existence of metastable (isomeric) states in nuclei allows for a very sensitive study of the reaction products and thus the reaction process itself. The fragments can be separated and identified, and their decays investigated in essentially background free conditions. The technique is often used to gain access to the structure of exotic nuclei [14–16], as well as for angular momentum population studies [17]. Here we will use isomeric decays in a novel way, namely to disentangle different contributions to the mechanism of relativistic heavy-ion collisions. The influence of nucleonic excitation on the population of excited states is suggested.

*Experimental details:* A primary $^{56}$Fe beam at an energy of $E/A$=500 MeV was provided by the SIS-18 accelerator at GSI, Darmstadt, Germany. The $^{56}$Fe ions impinged on a 662 mg/cm$^2$ $^9$Be target. The reaction products of interest were selected and identified in flight on an event-by-event basis by the FRagment Separator (FRS) [18]. The FRS was optimised for the transmission of bare $^{54}$Fe ions. The identification of the fragments was done by magnetic rigidity and energy loss measurements [19]. The transmitted and identified ions were slowed down in a variable thickness aluminium degrader and finally implanted in a passive plastic stopper. A total of $6.8\times10^6$ $^{54}$Fe nuclei were identified. The delayed $\gamma$ rays correlated with the implanted ions were detected with the AGATA tracking array [20]. The stopper was positioned 15 cm downstream from the nominal centre of AGATA in order to increase detection efficiency [21].

The use of the thin production target ensured that the energy straggling in the target is minimal and, consequently, the momentum distribution of the fragments is determined by the reaction mechanism. The FRS was operated in achromatic mode with open slits, resulting in 100% optical transmission for the centred $^{54}$Fe ions.

*Results:* The parallel momentum distribution of fragments can be deduced from their magnetic rigidity, that is from their physical distribution at the dispersive focal plane at the middle of the fragment separator. The parallel momentum distribution of the $^{54}$Fe fragments is shown in Fig. 1.

The delayed $\gamma$-ray spectrum associated with $^{54}$Fe is shown in Fig. 2. Several $\gamma$ rays are observed, which originate from the decay of the well known $T_{1/2}$=364(7) ns $I^\pi$=$10^+$ isomeric (metastable) state [24, 25].

The isomeric ratio, $IR$, is defined as the probability that in the reaction a nucleus is produced in an isomeric state. It can be determined experimentally as: $IR = \frac{Y}{N_{imp}FG}$ , where $N_{imp}$ is the number of implanted ions, and $Y$ is the isomeric yield. $F$ and $G$ are correction factors for the in-flight isomer decay losses and the finite detection time of the $\gamma$ radiation, respectively. The isomeric yield is given by: $Y = \frac{N_\gamma}{\epsilon_{eff} b_\gamma}$, where $N_\gamma$ is the number of counts in the $\gamma$-ray line depopulating the isomer, $b_\gamma$ is the absolute $\gamma$-ray branching ratio, and $\epsilon_{eff}$ is the $\gamma$-ray detection efficiency. For more details see, *e.g.*, reference [19].

The isomeric ratio of the $10^+$ isomer in $^{54}$Fe was determined as a weighted average from the $\gamma$ rays at 411, 1130, 1408 and 3431 keV. Its overall value is quite small at 0.77(6)%. Its dependence on the transferred momentum in the reaction is shown in Fig. 3. To investigate its momentum dependence, only the statistical errors on

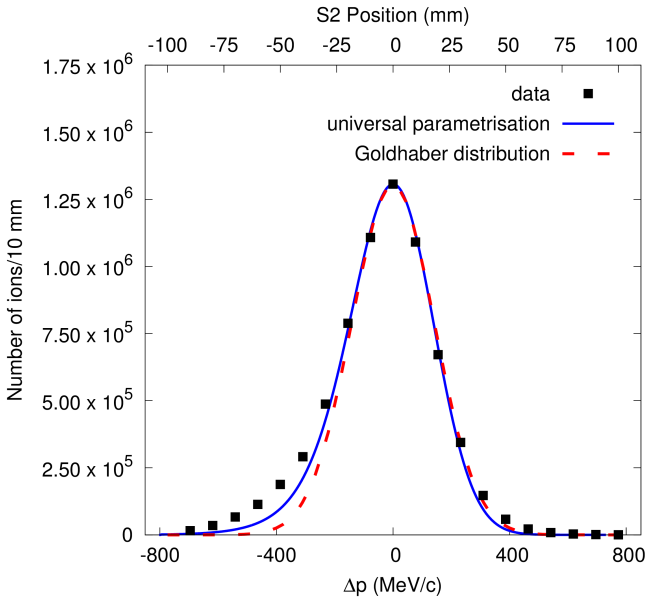


FIG. 1. Parallel momentum distribution of the $^{54}$Fe ions, as deduced from the position measurement (upper X axis) at the intermediate focal plane of the fragment separator. The measured distribution is compared with the universal parametrisation of [22] (continuous line) and a symmetric distribution as given by the Goldhaber formula [23] (dashed line).

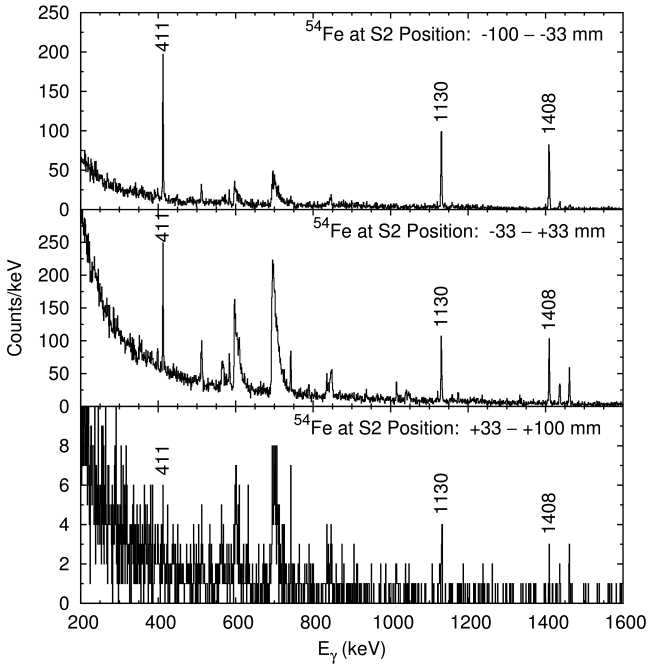


FIG. 2. Delayed ($\Delta t$=117–1960 ns) $\gamma$-ray spectrum associated with $^{54}$Fe. The three panels correspond to $^{54}$Fe ions with different parallel momentum ranges. *(top)* $\Delta p$= -750, -247 MeV/c (9.8x10$^5$ $^{54}$Fe ions); *(middle)* $\Delta p$= -247, +247 MeV/c (55.8x10$^5$ ions); *(bottom)* $\Delta p$= +247, +750 MeV/c (1.64x10$^5$ ions).

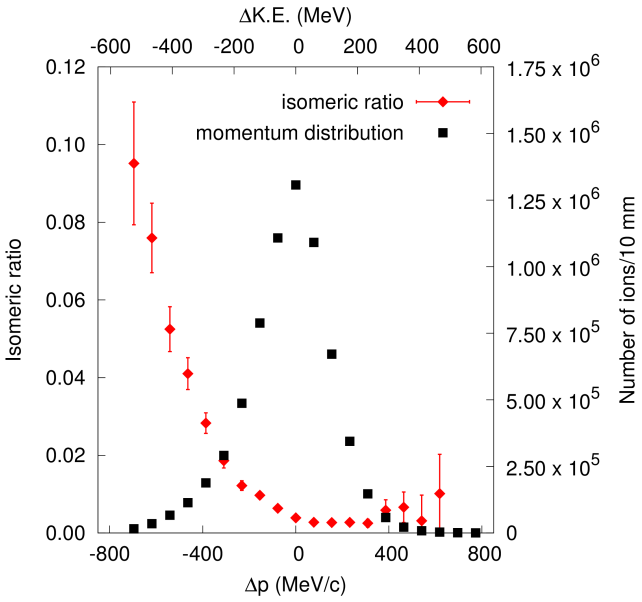


FIG. 3. Isomeric ratio of the 10$^+$ isomeric state in $^{54}$Fe as function of momentum transfer and corresponding kinetic energy loss (upper X axis). The measured parallel momentum distribution of the $^{54}Fe$ ions is also shown.

$N_\gamma$ are shown. The systematic errors, dominated by the absolute efficiency and the loss of $^{54}$Fe ions after identification due to reactions (estimated to be 20%), are around 10%, and affect all data points in the same way. The isomeric ratio is close to zero in the centre of the distribution and at positive momentum transfer to the fragment. However it is sizeable, in the order of several percent, at negative momentum transfer. The isomeric ratio increases with the amount of transferred parallel momentum.

*Discussion:* In relativistic-energy fragmentation the parallel momentum distribution is well understood, and it is determined by the removed nucleons. In the case of two particle removal, its width is connected to the angular momentum of the removed nucleon pair [26]. At high bombarding energies, such as in the present case, it is expected to be symmetrical [27, 28] around the zero momentum transfer. At lower energies there is a low momentum tail, understood as a contribution from deep-inelastic reactions. The size of the tail is dependent on the bombarding energy and it is larger at lower energies. The momentum distribution can be reproduced with the so called 'universal parametrisation', using parameters obtained from experiments [22].

As figure 1 shows, the experimental distribution measured here for $^{54}$Fe is close to symmetric, but there is an additional contribution, a tail, at negative momentum transfer. The tail is rather large for E/A=500 MeV bombarding energy. The aforementioned universal parametrisation predicts a very small tail, and so it is not able to reproduce the measured momentum distribution (see figure 1).

In fragmentation reactions, by removing two neutrons from the primary $^{56}$Fe beam, only two-neutron states can be populated in $^{54}$Fe. This is always the case, independently whether it is a direct two-neutron removal reaction or a neutron removal followed by the evaporation of a neutron, or even two consequent reactions in the thin target ($\sim 0.5\%$ of the events). The ground-state of $^{56}$Fe has zero angular momentum (spin). However the valence space does not contain enough angular momentum for two holes to create a state with spin $I$=10$\hbar$. Modern shell-model calculations include the full $pf$ shell, accounting for protons and neutrons up to $N = Z = 40$. Therefore, the maximum spin of two-neutron states is $I^{\pi}$=6$^{+}$ from the $\nu f_{7/2}^{-2}$ two-hole configuration. $I^{\pi}$=10$^{+}$ can be obtained first with two neutrons in the $\nu h_{11/2}$ orbital. This is in the upper part of the $N$=50–82 shell, and it is expected to be essentially empty. The $h_{11/2}^{2}$ component of the isomer can be estimated form the proton-decay of the analog 10$^{+}$ state in the mirror nucleus $^{54}$Ni, and it is in the order of $10^{-6}$ [29]. Consequently they play no significant role in the structure of the 10$^{+}$ isomer, and the production of this state requires at least four unpaired particles [29]. Therefore, it cannot be populated by fragmentation of $^{56}$Fe. The mechanism of populating the 10$^{+}$ isomer in $^{54}$Fe from $^{56}$Fe at relativistic energies has to be more complex.

The fragmentation and additional components of the relativistic-energy reaction reaction can be disentangled by considering that fragmentation has essentially a symmetric momentum distribution. The momentum distribution of $^{54}$Fe nuclei produced in additional reactions is shown in figure 4. It was obtained by subtracting the distribution of the universal parametrisation (shown in fig.1.) from the measured distribution. The large error bars are related to the uncertainty on where the middle of the measured distribution really is. An uncertainty of 1 mm was considered. As only the additional, non-fragmentation, reactions can produce the 10$^{+}$ isomer, the isomeric ratio is recalculated, and it is given on the same figure.

The non-fragmentation events show a maximum, at around momentum transfer $\Delta$p$\sim -400$ MeV/c, corresponding to $\sim -300$ MeV kinetic energy shift. The isomeric ratio increases at high momentum transfer. At the low momentum transfer side, the accuracy is not enough to distinguish between a raising or flat behaviour. Independently of whether the measured ion distribution is compared to the universal parametrisation (as shown in Fig. 4), the symmetric distribution of the Goldhaber formula or the measured positive-momentum side of the distribution, the same picture is obtained.

In the simple abrasion-ablation picture of the fragmentation, no products with more neutrons or protons than the projectile can be produced. However, experiments show that this happens even at very high, $E/A$=1 GeV, bombarding energy where the deep-inelastic reactions are negligible [6]. For example, $Z$=83 Bi isotopes [30] and $N$=127 isotones [31] were produced from $^{208}$Pb projectiles. There are two different mechanisms at play here: (i) quasielastic collisions where a proton (neutron) takes over the total kinetic energy of a neutron (proton), and (ii) excitation of a proton (neutron) into a $\Delta$(1232)-resonance state and its subsequent decay into a neutron (proton) via pion emission. The first mechanism does not modify the momentum of the fragment, while the second one reduces it due to the escaping pion, providing a way to disentangle the two processes experimentally [30, 32]. Both of these processes can result in a reaction product with higher number of protons (or neutrons) than the initial ion. Therefore we refer to these as non-fragmentation reactions. The charge pick-up cross section is in reasonable agreement with the prediction of the intranuclear cascade model [33], which accounts for $\Delta$ production and its decay via pion emission. However, the population of individual excited states cannot be predicted in that model because the nuclear structure is treated in a rather rudimentary way – no shell structure is considered.

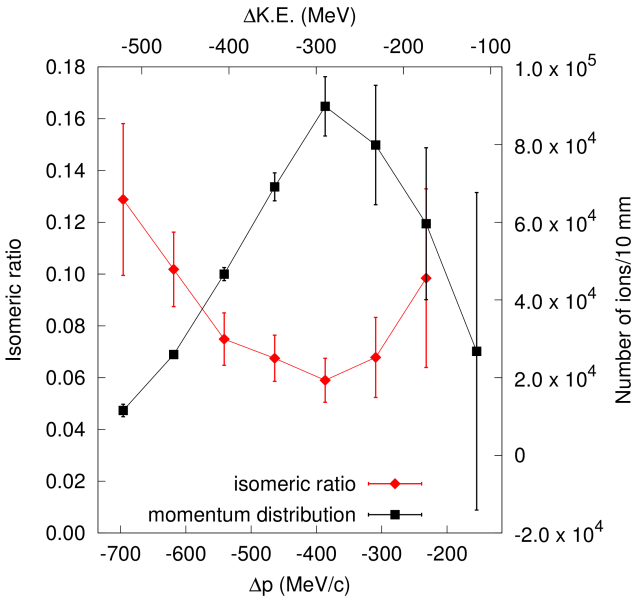


FIG. 4. Isomeric ratio of the 'non-fragmentation' part of the reaction, after the pure fragmentation events are removed, as a function of momentum transfer. The momentum distribution of the non-fragmentation events is also shown. The upper scale shows the corresponding kinetic energy shift.

In addition to fragmentation, $^{54}$Fe ($Z$ = 26) can be produced also via the above processes, from $^{55}$Co and $^{56}$Co ($Z$ = 27) prefragments. We note that the charge pick-up reaction cross section is energy dependent [30] and it is at its highest at energies around $E/A$ =500 MeV, the energy used in the present experiment. All processes identified to populate the nucleus $^{54}$Fe are illustrated in Fig. 5. The ones which involve excitation of the $\Delta$(1232) resonance produce fragments with lower momentum, so they can readily account for the observed tail in the distribution. Also, while the main fragmentation process cannot populate four-particle states, the

ones going through the $^{55,56}$Co prefragments can.

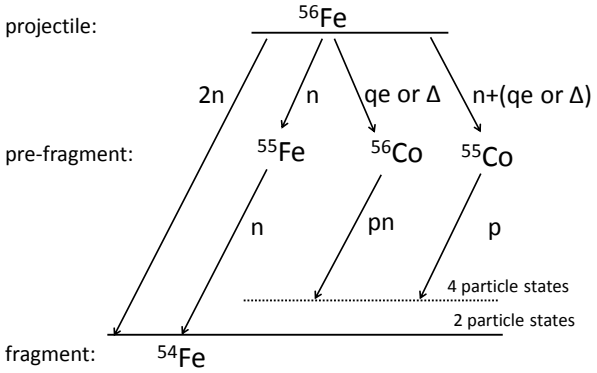


FIG. 5. Different reaction mechanisms populating $^{54}$Fe from a relativistic-energy collision of $^{56}$Fe. Only those proceeding through the $^{55,56}$Co pre-fragments can populate four particle states. The ones involving the $\Delta(1232)$ resonance result in a decreased momentum of the fragment. *qe* stands for quasielastic reaction.

The $^{55,56}$Co prefragments can either decay via $\gamma$ transitions to form $^{55,56}$Co fragments or evaporate particles. In the latter case, proton evaporation, leading to iron isotopes, is favoured as the proton separation energy is smaller by a factor of about two than the neutron separation energy in this neutron-deficient region of the nuclidic chart. The production cross section for both $^{55}$Co and $^{56}$Co is calculated within the Intranuclear Cascade Model [13, 33] to be around 3–4 mb, and we might assume a similar population probability of $^{54}$Fe from both $^{55}$Co and $^{56}$Co. The $^{54}$Fe production cross section from fragmentation is calculated to be 29.5 mb by the Intranuclear Cascade Model [13, 33], in good agreement with the 27.9 mb of the EPAX 3.1a parametrisation [34]. The measured experimental ratio of momentum tail and symmetric momentum distribution of $^{54}$Fe is $\approx$ 7–10%, in qualitative agreement with the above estimates. The average energy removed by the pion from the nucleus is around 300 MeV [6, 30, 35]. This value is in agreement with the measured energy loss of the fragment (see the secondary horizontal axis on Fig. 4).

It was previously observed that the population of high angular momentum states, $I > 15\ \hbar$, is higher than expected from fragmentation models [17, 36, 37]. However the models do not consider nucleonic excitations. As shown in the present example, excitations of the $\Delta$ resonance (and possibly other higher-lying resonances) and its subsequent decay can produce additional angular momentum in the final fragment. This might account for the increased population of high-angular momenta states even in nuclei where there are enough valence nucleons from the start.

*Conclusions:* The $I^{\pi}$=$10^{+}$ isomeric state of $^{54}$Fe was populated in the fragmentation of a $^{56}$Fe beam at an energy of $E/A$=500 MeV. This state has a four-nucleon configuration. Therefore, it cannot be populated by two neutron removal reactions. The isomer was populated in the low-energy tail of the $^{54}$Fe distribution. The population of the isomer can be explained by considering inner excitations of a neutron, the $\Delta$ resonance. Other, higher-lying resonances might also play a role. The removed pion accounts for the lower kinetic energy, while in the process additional valence nucleons are created, contributing to the four-nucleon nature of the isomeric state.

The present result opens up the possibility to study the final nuclear states following the decay of in-medium $\Delta(1232)$ and other higher-lying resonances in relativistic-energy heavy-ion collisions. The resonance production as well as the quantum state of the resulting nucleon after pion emission is expected to depend on the projectile as well as its energy. The existence of a large number of metastable states [38, 39] allows the extension of the present work to other regions of the nuclidic chart. Experiments focusing on nuclei with the same atomic mass as the projectile are the most promising as these allow the direct investigation of the process, without the interference caused by additional neutron or proton emission.

Acknowledgements: We thank the GSI accelerator staff for their excellent work. Fruitful discussions with J.A. Tostevin, E.C. Simpson and P.M. Walker are acknowledged. This work is supported by the STFC(UK), the Swedish Research Council, The German BMBF under grants no. 05P15RDFN1 and 05P12RDFN8, MINECO, Spain, under the grant FPA2014-57196-C5, Generalitat Valenciana, Spain, under the grant PROMETEOII/2014/019 and by the FEDER funds of the European Commission. This work has been supported by the European Community FP7 - Capacities, contract ENSAR No. 262010."

[1] L.W. Alvarez, F. Bloch¡ Phys. Rev. **57**, 111 (1940).
[2] R. Frisch and O. Stern, Zeits. f. Physik **85**, 4 (1933).
[3] M. Gell-Mann, Phys. Lett. **8**, 214 (1964).
[4] G. Zweig, Developments in the Quark Theory of Hadrons **1**, 22 (1980).
[5] J. Beringer et al. (Particle Data Group), Phys. Rev. D **86**, 010001 (2012).
[6] D. Bachelier *et al.*, Phys. Lett. B **172**, 23 (1986).
[7] Y. Ichigawa *et al.*, Nature Phys. **8**, 918 (2012).
[8] C.B. Hinke *et al.*, Nature **486**, 341 (2012).
[9] D. Steppenbeck *et al.*, Nature **502**, 207 (2013).
[10] M. Thoenessen, B.M. Sherill, Nature **473**, 25 (2011).

[11] R. Bernas, E. Gradsztajn, H. Reeves, E. Schatzman, Annals of Phys. **44**, 426 (1967).
[12] J.J. Gaimard, K.H. Schmidt, Nucl. Phys. A **531**, 709 (1991).
[13] A. Boudard, J. Cugnon, J.-C. David, S. Leray, D. Mancusi, Phys. Rev. C **87**, 014606 (2013).
[14] R. Grzywacz *et al.*, Phys. Lett. B **335**, 439 (1995).
[15] M. Pfützner *et al.*, Phys. Lett. B **444**, 32 (1998).
[16] Zs. Podolyák *et al.*, Phys. Lett. B **491**, 225 (2000).
[17] Zs. Podolyák *et al.*, Phys. Lett. B **672**, 116 (2009).
[18] H. Geissel *et al.*, Nucl. Inst. Meth. B **70**, 286 (1992).
[19] M. Pfützner *et al.*, Phys. Rev. C **65**, 064604 (2002).
[20] S. Akkoyun *et al.*, Nucl. Instrum. Meth. **668**, 26 (2012).
[21] N. Lalović *et al.*, Nucl. Inst. Meth. A **806**, 258 (2016).
[22] O. Tarasov, Nucl. Phys. A **734**, 536 (2004).
[23] A.S. Goldhaber, Phys. Lett. B **53**, 306 (1974).
[24] D. Yan, J. Huo, Nucl. Data Sheets **121**, 1 (2014).
[25] E. Dafni, J.W. Noé, M.H. Rafailovich, G.D. Sprouse, Phys. Lett. B **78** 1 (1978).
[26] E.C. Simpson, J.A. Tostevin, D. Bazin, A. Gade, Phys. Rev. C **79** 064621 (2009).
[27] E.C. Simpson, J.A. Tostevin, Zs. Podolyák, P.H. Regan, S.J. Steer, Phys. Rev. C **82**, 037602 (2010).
[28] E.C. Simpson, J.A. Tostevin, Zs. Podolyák, P.H. Regan, S.J. Steer, Phys. Rev. C **80**, 064608 (2009).
[29] D. Rudolph *et al.*, Phys. Rev. C **78**, 021301(R) (2008).
[30] A. Kelić *et al.*, Phys. Rev. C **70**, 064608 (2004).
[31] A.I. Morales *et al.*, Phys. Rev. C **84**, 011601(R) (2011).
[32] C. Gaarde, Annu. Rev. Nucl. Part. Sci. **41**, 187 (1991).
[33] D. Mancusi, A. Boudard, J. Cugnon, J.-C. David, P. Kaitaniemi, S. Leray, Phys. Rev. C **90**, 054602 (2014).
[34] K. Sümmerer, Phys. Rev. C **86**, 014601 (2012).
[35] T. Udagawa, P. Oltmanns, F. Osterfeld, S. W. Hong, Phys. Rev. C **49**, 3162 (1994).
[36] M. Bowry *et al.*, Phys. Rev. C **88**, 024611 (2013).
[37] A.M. Denis-Bacelar *et al.*, Phys. Lett. B **723**, 302 (2013).
[38] P.M. Walker, G.D. Dracoulis, Nature **399**, 35 (1999).
[39] A.K. Jain, B. Maheshwari, S. Garg, M. Patial, B. Singh, Nucl. Data Sheets **128**, 1 (2015).